



Thermally driven MEMS fiber-grippers

Mohammad S. Islam¹ · Sushmita Challa¹ · M. H. Yacin² · Sruthi S. Vankayala³ · Nathan Song⁴ · Danming Wei¹ · Jasmin Beharic⁵ · Cindy K. Harnett¹

Received: 30 November 2022 / Revised: 29 July 2023 / Accepted: 9 August 2023 / Published online: 24 August 2023
© The Author(s), under exclusive licence to Springer-Verlag GmbH Germany, part of Springer Nature 2023

Abstract

We investigate mechanical tangling for adhesion of microelectromechanical systems (MEMS) to unconventional carrier materials for assembly of highly porous, fiber-based electronics. Adhesion plays a crucial role in fabrication, but is a difficult task to realize even on continuous thin films of soft materials like silicone and polyimide. Adhesion becomes more challenging on discontinuous surfaces like fabric meshes, yet these substrates will expand the MEMS universe to new materials. Operations that are challenging on conventional circuit boards, like passage of electronic contacts and fluids from one side of a mesh to the other, are simpler with a mesh. In this work, microgripper arrays are realized by microfabrication and release of strained metal-oxide bilayers. This paper describes a process that wraps a MEMS gripper around a conductive fiber and reverses the process using electric current to open the gripper. The gripper's electrical resistance serves as a self-temperature sensor over the 20–500 °C range. Beyond their potential for adhering MEMS to fabrics and to flexible/stretchable substrates that are incompatible with or resistant to adhesives, these microgrippers illustrate how MEMS-based microrobots might interact with small-scale (< 200 μm diameter) soft and biological structures that require sub-millinewton contact forces. The key contribution of this paper over our earlier work is demonstrating the grippers' temperature-dependent resistance, which offers a route to improved control of the gripper state.

Keywords Thin film · Residual stress · Bimorph structure · MEMS microgripper · Thermal actuators

1 Introduction

Functional integration of heterogeneous materials can enable novel MEMS design formats to be implemented on substrates with characteristics such as stretchability, breathability, etc. The reversible geometric transformation of MEMS

realized through thermal actuation via pulsed current can allow this integration to be real-time configurable.

MEMS actuation can enable scheduled release of environmental samples from microcontainers for analysis [1], while other MEMS based mechanical devices detect fluid flow events [2], steer and modulate light, produce three

✉ Mohammad S. Islam
shafquatul.islam@louisville.edu

Sushmita Challa
sushmita.challa@louisville.edu

M. H. Yacin
myassin3@illinois.edu

Sruthi S. Vankayala
sruthisarani93@gmail.com

Nathan Song
nathansong@berkeley.edu

Danming Wei
danming.wei@louisville.edu

Jasmin Beharic
jasmin.beharic@louisville.edu

Cindy K. Harnett
cindy.harnett@louisville.edu

¹ Electrical and Computer Engineering, University of Louisville, Louisville, KY, USA

² Materials Science and Engineering, University of Illinois at Urbana-Champaign, Urbana, IL, USA

³ Computer Science Engineering, Gayatri Vidya Parishad, Visakhapatnam, India

⁴ Department of Physics, University of California, Berkeley, Berkeley, CA, USA

⁵ Micro-Nano Technology Center, University of Louisville, Louisville, KY, USA

dimensional electric fields in microfluidics and other applications, and serve as electromagnetic resonators, antenna elements and probes for observing surface topology in atomic force microscopy [3].

Understanding the electrical and mechanical characterization of MEMS microgripper actuation can enable dynamic formatting of functional gripper contacts with fiber substrates. Decision parameters such as electrical contact area, mechanical clasp strength, and latching-unlatching with the fiber can be controlled by electrical switching between the various stable states of gripper actuation. These actuating MEMS fiber grippers can have a wide scope of applications in microrobot technology as fiber crawlers carrying payloads [4]. Contemplating locomotion, micro assembly and micromanipulations on fiber systems helps envision biological vessel networks for microsurgery [5], textile circuit routing [6], electronic textile fabrication [7] and tissue engineering [8].

Various methods realizing MEMS actuation have been demonstrated in literature such as, actuation triggered by light [9], fluid flow, electrothermal actuation [1, 2], electrostatic actuation [10], electromagnetic actuation [11] and piezoelectric actuation [12]. The electro-thermal actuators can be further classified based on the basis of in-plane and out-of-plane actuation. While U-beam/hot-and-cold-arm actuators [13] and V-beam/chevron actuators [14] are employed for horizontal/lateral actuation, the bimorph actuators in this work and others [15] are used for out-of-plane actuation. MEMS actuators can be bilayer [16], trilayer [17] or multimorph structures implemented with materials with differential expansion. MEMS researchers have demonstrated bilayers of metal/diamond like carbon or metal/oxide, and trimorphs of metal/polymer/oxide for applications in medicine [18]. Bimorphs of Al/SiO₂ [19], and Cu/W [20] have been used to implement micro-mirrors.

In this work we characterize the fiber gripper actuator response in terms of resistance, temperature, and radius of curvature of the device with respect to current applied at the contact pads. We envision the gripper clasping and detaching from the fiber, and put forth insights of the gripper actuator carrying payloads.

2 Methods

2.1 Theoretical analysis methods

The MEMS microgripper is designed to have 12 gripper arms of length 740 μm built in a continuous trace format (Fig. 1) where one of the arms is fixed and connected to contact pads. The gripper's arm trace width is 10 μm and its contact pads

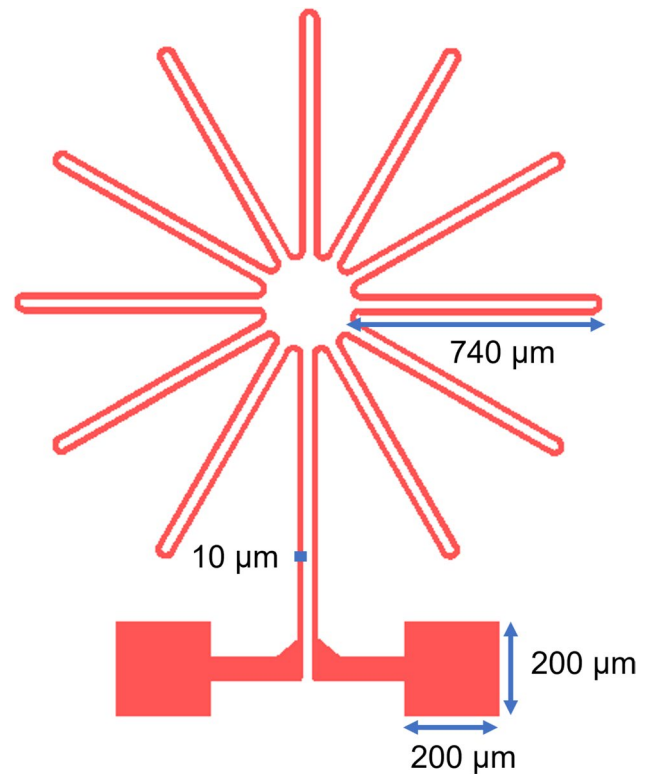


Fig. 1 Bimorph MEMS microgripper design

dimensions are 200 μm * 200 μm for the purpose of electrical probing for driving current and enabling thermal actuation. A donut-shaped etch window of 1850 μm outer diameter and inner diameter 330 μm encompassing the gripper is designed such that the gripper center is fixed to the substrate. The bimorph microgripper curls to a radius of curvature ρ when released from the surface due to differential thermal expansion of the bilayers. This is the radius that a working gripper gets to when no current is applied. The curvature, or inverse radius $1/\rho$, is given by Eq. 1:

$$\frac{1}{\rho} = \frac{6\epsilon(1+m)^2}{d[3(1+m)^2 + (1+mn)\{m^2 + (mn)^{-1}\}]} \quad (1)$$

where ϵ is the strain mismatch or fractional difference in the unconstrained relaxed lengths of the two layers $(l_B - l_A)/l_o$, d is total thickness ($d = d_A + d_B$), n is the ratio of the elastic modulus of the layers, ($n = E_A/E_B$) and m is the ratio of their thicknesses ($m = d_A/d_B$). Subscripts 'A' and 'B' refer to the upper metal and lower oxide layers, respectively.

$$\frac{1}{\rho} = \frac{6(\alpha_B - \alpha_A)(t - t_o)(1+m)^2}{d[3(1+m)^2 + (1+mn)\{m^2 + (mn)^{-1}\}]} \quad (2)$$

If $d_A = d_B$ then $m = 1$

$$\frac{1}{\rho} = \frac{24(\alpha_B - \alpha_A)(t - t_o)}{d \left[14 + n + \frac{1}{n} \right]} \tag{3}$$

If $m = 1$ and $n = 1$ that is $E_A = E_B$ and $d_A = d_B$

$$\frac{1}{\rho} = \frac{3(\alpha_B - \alpha_A)(t - t_o)}{2d} \tag{4}$$

Equation 1 could also be represented as Eqs. 2, 3, 4 where t_o is the initial temperature of the gripper, t is the temperature at which the gripper starts to actuate. These equations are useful in obtaining the theoretical radius of curvature of the microgripper actuation for a given thermal condition (applied current).

The strain mismatch is induced by thermal expansion during fabrication, causing the layers to curl up from the substrate at room temperature. When the structure is heated, it opens and flattens, because the top metal layer has a more than 50 times greater thermal coefficient of expansion (TCE) than the oxide layer. T_f describes the “flat temperature” at which the released pop-up MEMS will become planar again:

$$T_f \approx T_o + \frac{\Delta T_B(\alpha_{si} - \alpha_B) - \Delta T_A(\alpha_{si} - \alpha_A)}{(\alpha_A - \alpha_B)} \tag{5}$$

where (in standard SI units) T_o is liftoff temperature (room temperature), ΔT_B is oxide deposition temperature - liftoff temperature, ΔT_A is metal deposition temperature - liftoff temperature, α_{si} is silicon TCE, α_A and α_B are metal and oxide TCE, respectively. With increasing current through the metal layer, gripper temperature increases (Fig. 2b).

2.2 Finite element analysis methods

A finite element modeling (FEM) simulation was carried out using COMSOL Multiphysics 5.5 software to analyze the mechanical deformation behaviors of the Au/SiO₂ microgripper due to applied voltage. The microgripper was modeled in accordance with the design dimensions discussed earlier and using original material properties provided in COMSOL material library. Following the construction of the model geometry, material properties are added to the bilayer structure with the top layer chosen as Au, while the bottom layer is assigned to SiO₂. For each microgripper arm the anchored surfaces around the center of the microgripper for both Au and SiO₂ layers were assigned to have mechanically fixed surface boundary conditions while other surfaces were kept free to move in the Structural Mechanics module. The finite element simulations were performed using physics-controlled meshing elements with a linear solver. Electric potential ranging from 0 to 1.5 V is applied on the fixed arm of the microgripper which is connected to the contact pads as presented in Fig. 1. This applied voltage induces an

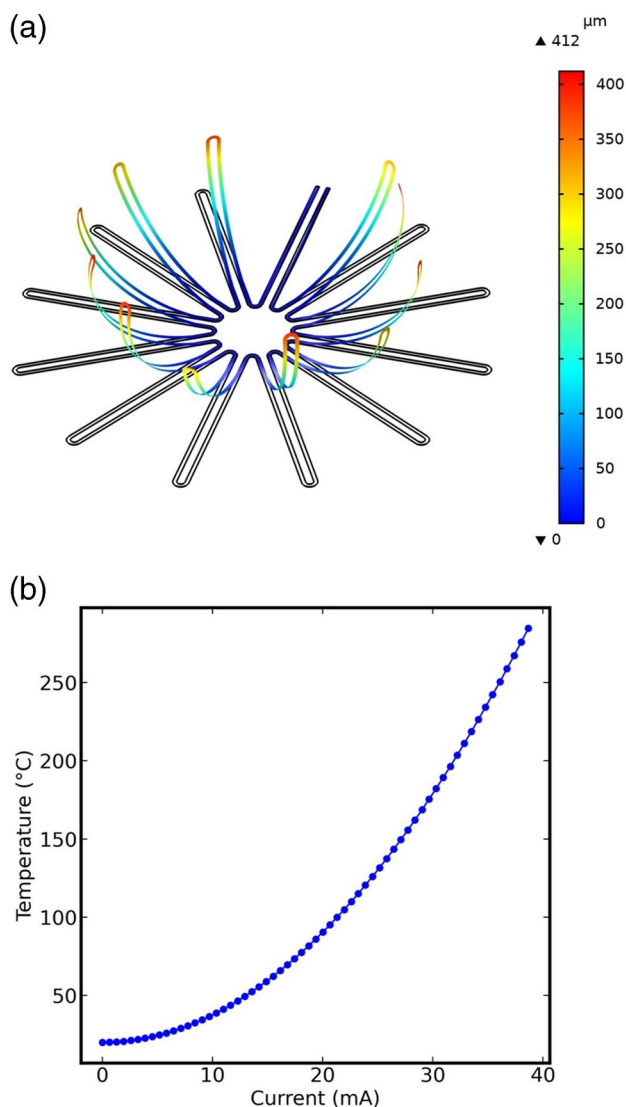


Fig. 2 FEM simulation of the microgripper: **a** deformation with temperature-dependent electrical conductivity; **b** Temperature of the microgripper top layer (Au) for different values of applied current

electric current and due to the material’s resistivity, in this case Au, the current heats up the structure. The thermally induced stress loads the material and deforms the microgripper arms.

By using the Joule Heating and Thermal Expansion pre-defined multiphysics interface, COMSOL automatically adds the equations for three physics including the necessary multiphysics couplings. COMSOL modules, Heat Transfer and Structural Mechanics, work in conjunction to model the mechanical deformation and performance of the microgripper structure as a function of temperature which is dependent on the voltage applied. Figure 2a illustrates maximum gripper tip displacement of 412 μm resulting from an applied voltage of 1.5 V. The numerical results of the simulated temperature as a function of applied current are presented in Fig. 2b.

2.3 Fabrication methods

The bimorph actuator is fabricated on the Si substrate by depositing strain mismatched layers of different thermal expansion coefficients. A 450 nm thick SiO_2 coating is thermally grown on a silicon wafer by wet oxidation at 1000 °C. The oxidized wafer is coated with Shipley 1813 photoresist, and the wafer is exposed on a contact aligner (Karl Suss) to ultraviolet (UV) light through a bright field mask. Image reversal using a Yes oven is carried out followed by flood exposure at the aligner and a development step in MF319 developer. The image reversal process makes the photoresist sidewalls slanted assisting in small features clearing in the lift off process. A Ti-Au metal layer of 480 nm combined thickness (where Ti and Au are 10 and 470 nm, respectively) is deposited on the wafer using a sputtering machine (Lesker PVD75). A lift-off process is carried out in acetone to obtain the metal patterned oxidized wafer. A second photolithography patterning is carried out using a dark field mask containing the torus shaped etch window design. Plasma assisted selective oxide removal is done in a reactive ion etch chamber (March) for about 10 min with 300 mTorr pressure of $\text{CF}_4:\text{H}_2$ at a partial pressure ratio of 50:3 and a RF power of 300 W. The overall microgripper fabrication process flow is illustrated in Fig. 3. The processed wafer is then diced, and

each die is wire bonded to a printed circuit board as shown in Fig. 4. A single tinned Cu wire (Karl Grimm) is aligned to the gripper with a tolerance of 400 microns. An isotropic

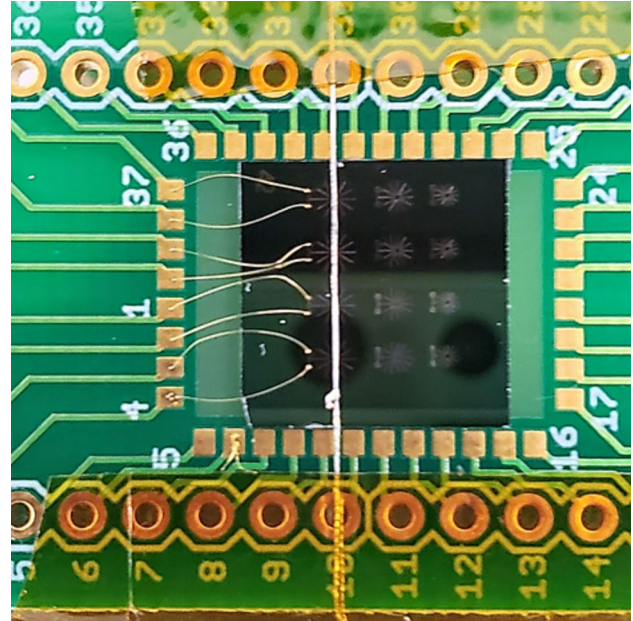


Fig. 4 Fabricated device wire bonded to a printed circuit board

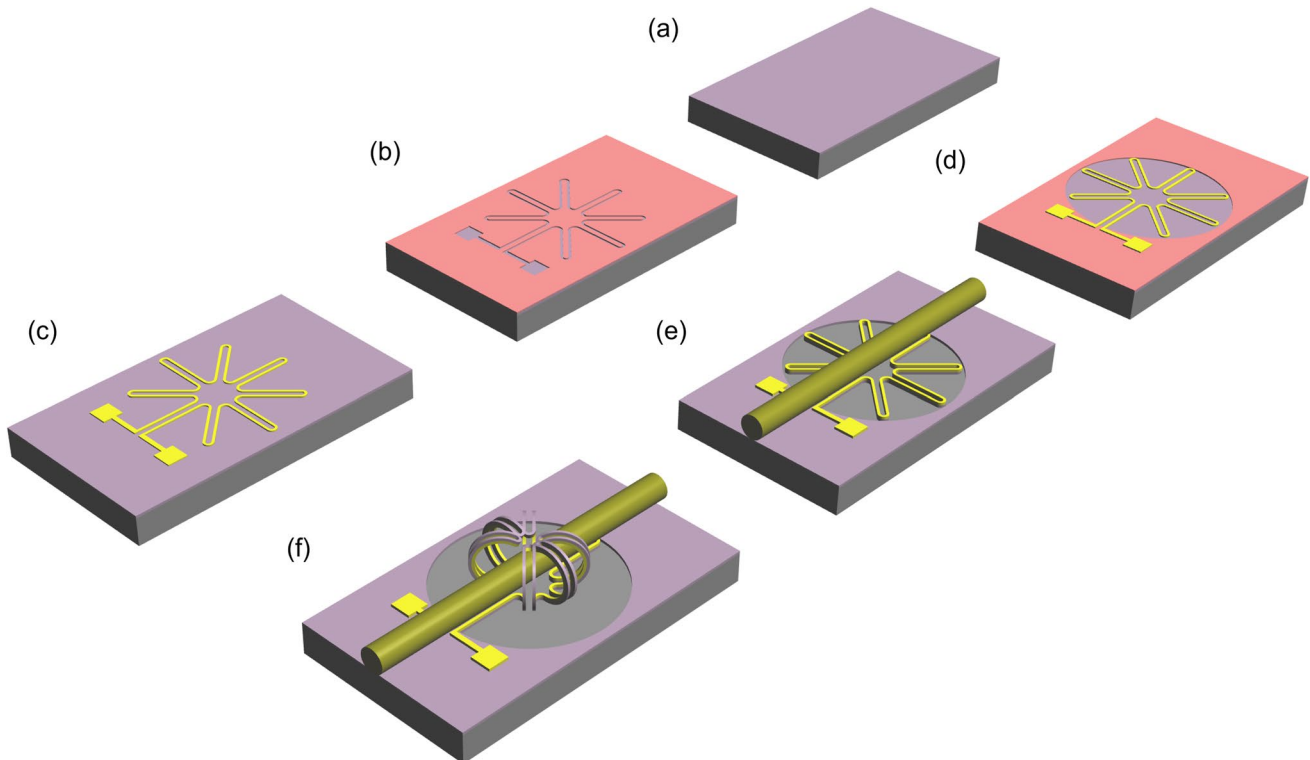


Fig. 3 Microgripper Fabrication Process Flow: **a** 450 nm SiO_2 deposited on Si wafer; **b** Photoresist patterning carried out using Yes oven with gripper design mask; **c** 470 nm Au-Ti sputtering and lift-off

using acetone; **d** Photoresist patterning for selective etch windows; **e** SiO_2 plasma etch and fiber-tinned Cu alignment; **f** Dry silicon etch to release bimorph actuator arms from the substrate

XeF₂ assisted Si etch is carried out using Xactix to release the MEMS gripper arms from the substrate, keeping the center of the device and contact pads attached to the wafer.

2.4 Device characterization methods

Fabricated bimorph cantilever array diced into wafer dies were placed onto a hot plate station to record the change in length (as seen from top-view) based on changes in temperature. The experimental setup is illustrated in Fig. 5. Optical measurements were taken by visual inspection of the actuators on-screen, with measurement error primarily coming from vibration of the hot plate stage. Optical measurements were recorded at different hotplate temperatures. These are cantilevers not microgrippers, but they have been fabricated using the same process and yields the same radius of curvature as the microgripper arms.

When heated from 30 to 160 °C, these actuators displayed relatively ‘rigid’ behavior and there was no visible shaking from the hot plate vibrations. After this threshold (up until the limit of 210 °C), the actuators gradually became more responsive to minor vibrations.

This effect is prominent in the error bars of Fig. 8. Shaking the heating stage through manual adjustments revealed strong Hookean behavior at high temperatures.

3 Results

3.1 Gripper actuation results

The device behavior can be analyzed using the following results on gripper resistance, actuation current threshold, current handling capacity, electrical and mechanical insights on thermal actuation.

We tested 34 grippers (1000 μm diameter probing design gripper) for their average resistance when carrying 10 mA of current, the median value was 96 Ω +/- 31 Ω, within uncertainty of the theoretical value of 108 Ω; presented in Fig. 6. After testing 16 grippers (1000 μm diameter probing

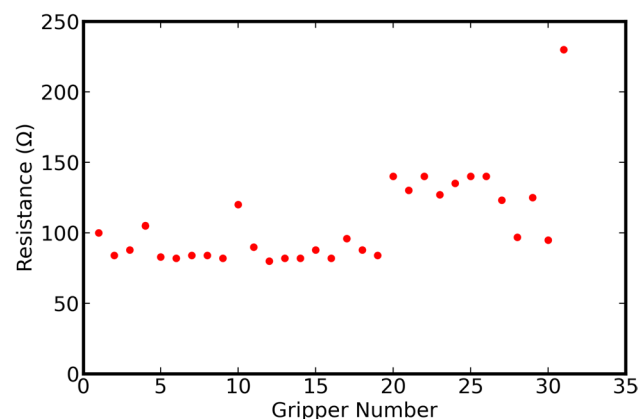
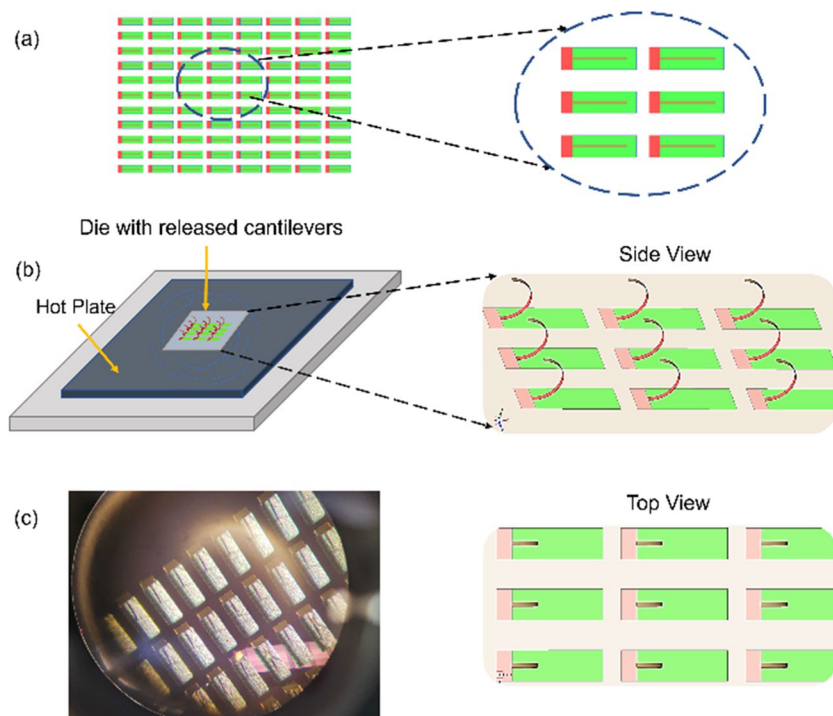


Fig. 6 Scatter plot of the measured resistance across different gripper devices at an applied current of 10 mA

Fig. 5 a L-Edit design of bilayer cantilever array (300 μm * 15 μm) – representing flat cantilevers before release; b Die consisting released cantilever array placed on a hot plate; c Top view image of released devices – microscopic image (left), schematic representation (right)



design gripper) for their maximum current density, the median value was 40 mA: vastly superior to the theoretical value of 9.4 mA.

Although theoretical, the best temperature approximation where the metal and oxide flatten after release (Eq. 2) is 337 °C (based on a metal deposition temperature of 200 °C). A model extrapolating the flat temperature vs. metal deposition temperature (both above and below 200 °C) shows a linear trend.

Pop-up MEMS begin to ‘unfold’ perceptibly at approximately 6.5 mA. Grippers can handle 1 mA of current for 8.5 min uninterrupted. Figure 7 shows the thermal actuation of the fiber gripper at various levels of applied current. Working out the gripper actuation at lower currents and small step increments can increase the repeatability and actuation life of the gripper. The present Au-Pt devices can handle up to 50 mA of current without burning out compared to our previous devices made out of Cr/Ni/Cr and Ti/Pt that could handle only 3 mA and 18 mA of currents, respectively [21]. From our previous experiments, the gripper cools down to room temperature in vacuum (change of state) in 10 ms as an upper limit measured by SEM frame rate. The previous Cr/Ni/Cr and Ti/Pt devices could sustain 1000 cycles of state change. With the current gripper design with Au-Pt layers, we observed that higher the initial current induced and the longer amount of time it is induced, the smaller number of iterations the gripper can be re-used. In

the future work we wish to employ devices with thin layer of Au over Cr, so that the electrical properties do not dominate the desired mechanical characteristics.

At room pressure and temperature, we cooled the devices by convection, placing an electric fan 30 cm from the devices while running current through the gripper. We observed that the fan reduced the measured resistance from 87.5 ohms to 61 ohms.

3.2 Radius of curvature versus temperature

We tested 45 single gripper arms or cantilevers for their radius of curvature as temperature was varied. Despite large variance in individual grippers, an overall trend was modeled using the averaged results. The radius of curvature of our gripper clasps should theoretically agree with Eq. 2. Using an initial approximation of α_B (SiO₂) value as $0.65 \times 10^{-6} \text{ } ^\circ\text{C}^{-1}$, the calculated values in Table 1 were obtained. Table 1 shows the theoretical values for variables used in Eq. 2 and the calculated values within the theoretical range represented by the predicted values in Fig. 8. Allowing for tolerances of <5% for our parameters*, we observe that our values lie within the theoretical bound of our model.

Figure 8 shows Eq. 2 fitted to our calculated values as ‘Predicted Values’, with the tolerance bands represented in the ‘Error Bound’ range. The experimental values are shown

Fig. 7 Current loaded micro-gripper thermal actuation: **a** gripper at 5 mA applied current; **b** gripper unfolding at 15 mA; **c** gripper unfolding at 25 mA; **d** gripper at 35 mA

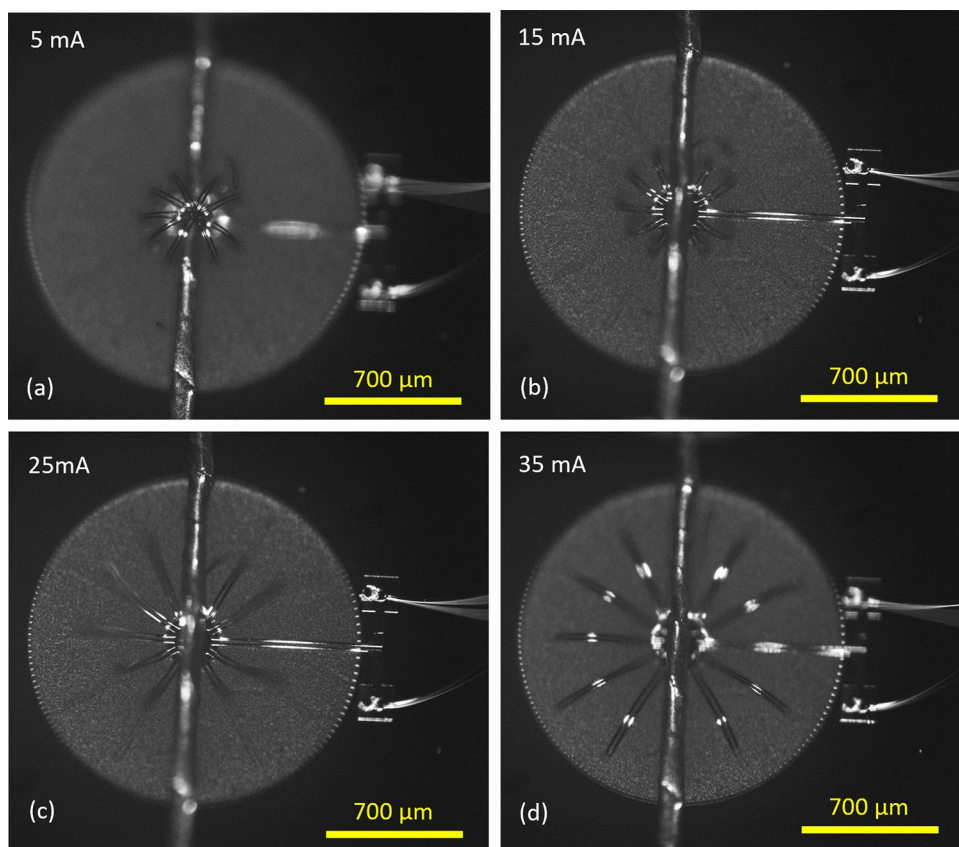


Table 1 Theoretical and calculated values for variables in Eq. 2

Variables	Theoretical	Calculated
α_A	$13.8 \sim 22.6 \times 10^{-6} \text{ }^\circ\text{C}^{-1}$ [22]	$20.66 \times 10^{-6} \text{ }^\circ\text{C}^{-1}$
α_B	$0.55 \sim 1 \times 10^{-6} \text{ }^\circ\text{C}^{-1}$ [22]	$0.65 \times 10^{-6} \text{ }^\circ\text{C}^{-1}$
t_0	$\sim 337 \text{ }^\circ\text{C}$ **	329.04 $^\circ\text{C}$
d	$\sim 1 \text{ } \mu\text{m}$	0.875 μm

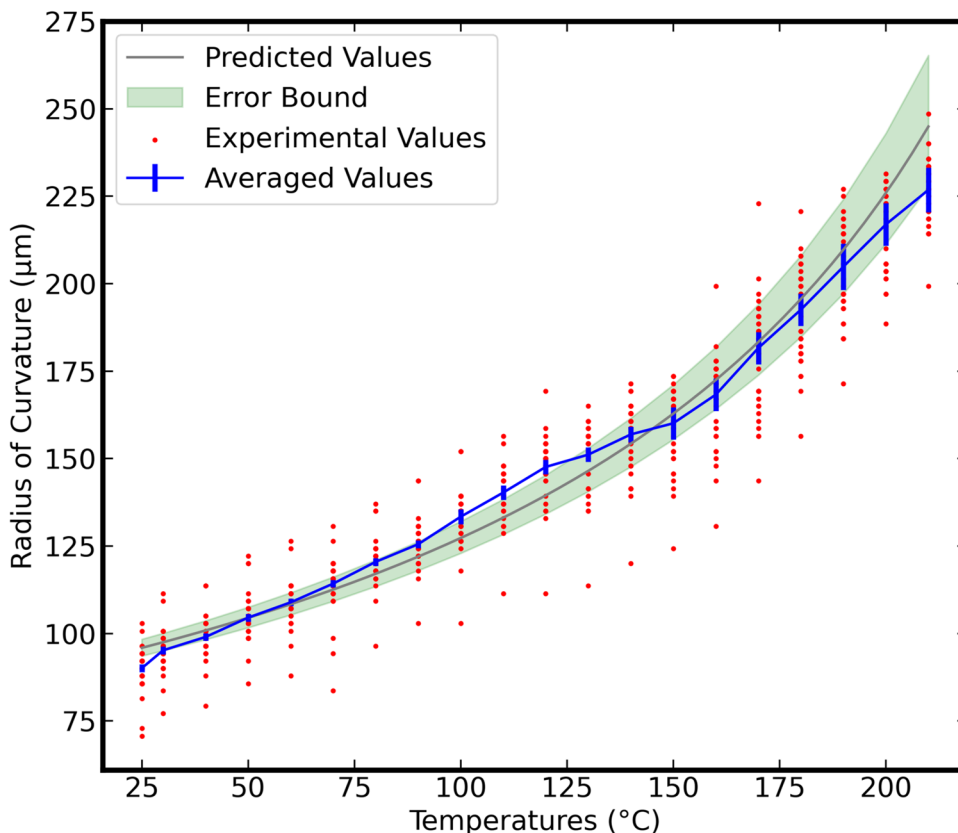
* Specifically, $\alpha_A \pm 1\text{e-}6 \text{ }^\circ\text{C}^{-1}$, $t_0 \pm 10 \text{ }^\circ\text{C}$, $d \pm 0.05 \text{ } \mu\text{m}$, $n \pm 2\%$, and $m \pm 3\%$

** This value is obtained by inserting $\alpha_A = 14 \times 10^{-6} \text{ }^\circ\text{C}^{-1}$, $\alpha_B = 0.71 \times 10^{-6} \text{ }^\circ\text{C}^{-1}$, $\alpha_{Si} = 3 \times 10^{-6} \text{ }^\circ\text{C}^{-1}$ in Eq. 5

for reference. Though many individual data points fall well outside the error bound (primarily due to manufacturing inconsistencies), our averaged values tended to stay within a 5–8% range.

The experimental flattening temperature (*radius of curvature* $\sim 0 \text{ } \mu\text{m}$) was at 329.04 $^\circ\text{C}$, supporting our model from the results presented in Section 3.1 that predicted 337 $^\circ\text{C}$. Experimental observations saw a large increase in measurement error beginning at $\sim 150 \text{ }^\circ\text{C}$, as shown in Fig. 8. Further increases in temperature only amplified this effect: small vibrations caused large, persistent gripper oscillations. This suggests that these grippers could be thought of as Hookean springs, with oscillations constrained in the direction of curvature.

Fig. 8 Actuator curvature versus temperature. Experimental results in red, given error bounds in green. Averaged values generally fall in bound



Combined with our qualitative observations, the results confirm the theoretical models and suggest that grippers have low rigidity at higher temperatures. We believe this may imply a lower gripper contact strength at temperatures greater than 150 $^\circ\text{C}$, which could be explored by stretching a fabric mesh with grippers latched on. This could also be a product of biaxial tension. Tension on the thin axis of the gripper arm that releases at the critical temperature could explain the sudden appearance of oscillatory behavior.

3.3 Radius of curvature versus current

The radius of curvature of the gripper clasp, contact area, and conformability with the fiber are determinants of adhesion. Some of previous gripper to fabric release results illustrate the successful transfer and adhesion of MEMS devices to discontinuous surfaces like fabric meshes as shown in Fig. 9. The firmness of the gripper clasp can be fine-tuned towards desired electrical and mechanical contact by understanding the variation of the gripper’s radius of curvature with applied current.

The radius of curvature of the top view gripper images at varying currents is obtained through a MATLAB binary and grayscale image analysis algorithm which detects data points on the outer circumference of the gripper. For all the grippers images at different currents (with gripper arms

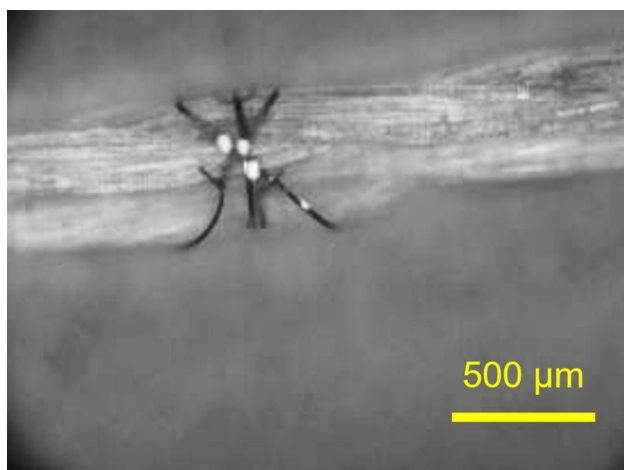
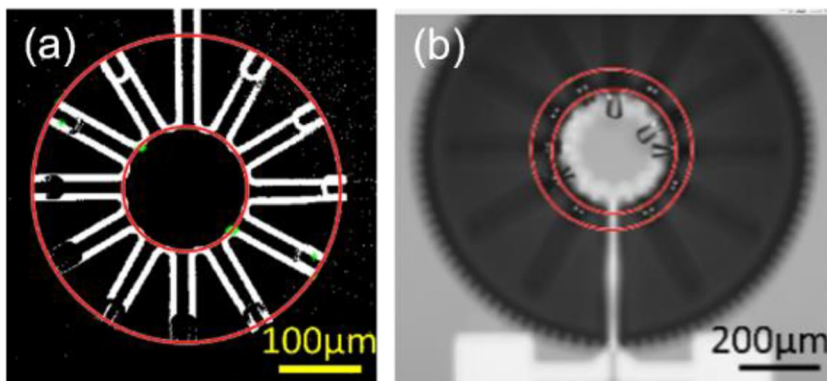


Fig. 9 Successful transfer and adhesion of grippers to a fiber

making $> 90^\circ$ and $< 90^\circ$ turns), we applied conditions for detecting outer circumference points at angles where gripper arms were drawn. These data points were averaged to find the mean radius.

The microgrippers in this work require an applied current of 6 mA or greater to actuate them. Currents ranging from 0 to 5 mA produced no visible effect on the gripper arms upon inspection under optical microscope. In order to ensure repeated use of these microgrippers one has to ensure that the applied current is active for less than 45 s during each run and current ranging between 0 and 25 mA. We noted that sending greater than 40–50 mA would cause the gripper to permanently open circuit, and at this point the gripper arms curled more than the theoretical value of radius of curvature of a working gripper presented in Fig. 10b. The MEMS micro-hotplate literature has shown that thermal stresses in current-carrying thin metal films can damage SiO_2 underlayers [23]; a similar mechanism is likely at work here. Trigonometry was used to calculate the radius of curvature from the projected length and the known arclength of the gripper arm. Using $r = L/\theta$, where $L = 740 \mu\text{m}$, the radius of curvature was deduced. In Fig. 10a the gripper has radius of curvature of $146 \mu\text{m}$. Here, the microgripper is at its resting

Fig. 10 Gripper radius of curvature for 740-micron long gripper arms **a** before carrying current; **b** after carrying 50 mA current



state after being released through microfabrication with no applied current. Figure 10b on the other hand, was subjected to 50 mA current and has a radius of curvature of $97 \mu\text{m}$.

Figure 11 shows the change in radius of curvature of the microgripper with respect to applied current. The blue plot shows the theoretical plot of applied current versus gripper radius of curvature derived from gripper radius versus temperature calculation from Eq. 2 and linear interpolation of the temperature values on the FEM model in Fig. 2b to obtain the corresponding current values. Also, the red plot shows the experimental data of radius of curvature along with standard deviation error bars at a given current obtained using image processing algorithm discussed above.

3.4 Resistance versus temperature

Since the resistivity of most metals depend on temperature, we investigated the MEMS structures' function as resistive temperature sensors. Because radius of curvature depends on temperature, and temperature depends not only on current but on heat sinking by the surrounding environment, such self-temperature sensing will be useful in controlling the gripper's position. The current conductance happens through the upper Au metal layer of the bimorph. The positive temperature coefficient of resistivity of gold, indicates an increase in resistance with respect to increase in temperature due to applied current, which is shown in the theoretical plot of the graph Fig. 12. The resistance is calculated by multiplying the theoretical resistivity by l/a , where l is the total trace length of the gripper actuator, which is 15.8 mm, and a is the cross-sectional area, $5 \mu\text{m}^2$. The theoretical resistance and temperature values for gold are presented in Table 2.

On the experimental standpoint, currents in the range of 5–45 mA in steps of 5 mA were applied to the device and subsequent resistance values were noted. From the trend-line approximation of the theoretical curve, values for the temperature are obtained by linear interpolation into the curve at the measured resistance values (Table 3), and the experimental datapoints are plotted. Figure 12 shows how measured resistances were used to look up temperatures on

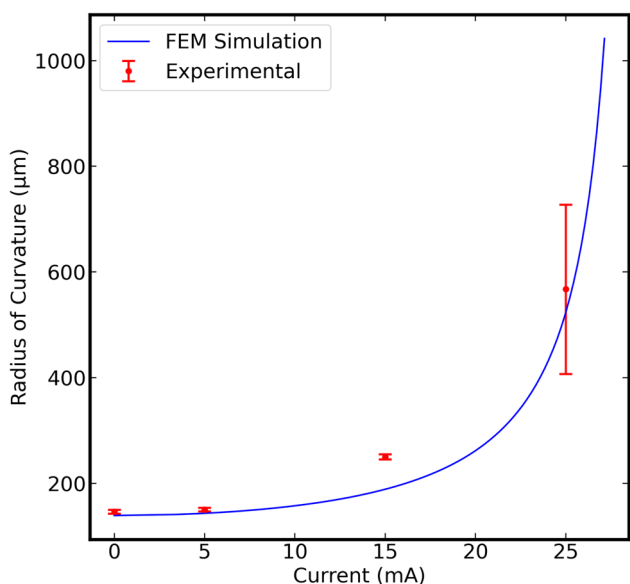


Fig. 11 Blue curve: Theoretical plot of applied current versus gripper radius of curvature derived from Eq. 2 and FEM model in Fig. 2b; Red points: Experimental data of radius of curvature at a given current obtained from image processing on gripper images from Fig. 7

the theoretical resistance-vs-temperature curve; temperature was not directly measured in this experiment. However, the resistance measurements were subject to instrument uncertainty, illustrated as vertical error bars on the experimental data points.

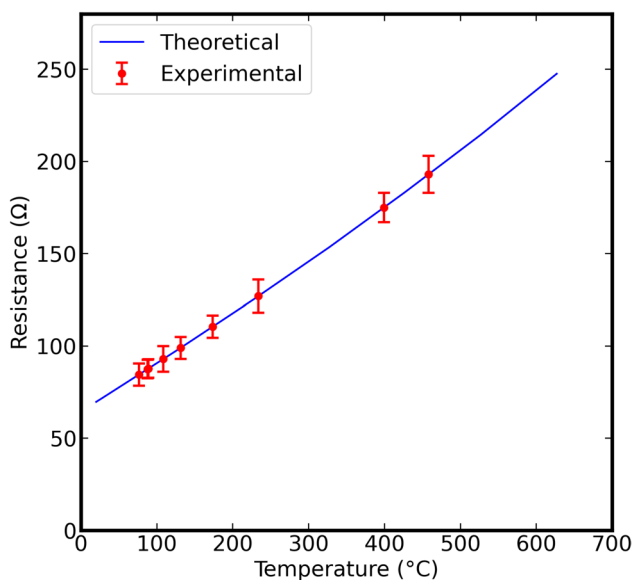


Fig. 12 Blue curve: Theoretical resistance versus temperature for the top metal layer (Au) of the biomorph structure; Red points: Experimental data of measured resistances for 5 to 45 mA applied currents in 5 mA increments, placed on theoretical resistance versus temperature curve

Table 2 Theoretical resistance and temperature data for gold

Theoretical T (°C)	$\rho(\times 10^{-8})$ (1/Ω)	Theoretical R (Ω)
20	2.22	69.74
25	2.26	71.03
27	2.27	71.54
127	3.11	97.87
227	3.97	125.06
327	4.87	153.41
427	5.82	183.33
527	6.81	214.52
627	7.86	247.59

3.5 Gripper interaction with fibers

Now we focus on how fibers influence the grippers’ configuration by exerting forces on the gripper arms. Figure 13 shows the SEM image of a released microgripper latching onto a fiber. Such a structure might connect a sensor or other device payload to a conductive fiber for power, actuation, or communication. The key to connecting payloads is ensuring payload and fiber compatibility with the MEMS fabrication and release process. The tinned copper wire in Fig. 13, added during fabrication (Fig. 3e), is unaffected by the highly selective XeF₂ release process. If applications require optimal contact the gripper radius can be matched to the fiber diameter (Fig. 7) by working out the theoretical parameters (Eqs. 1 and 2) to get the right radius during fabrication, and fine tuning of the contact area can be done after release by changing the actuation parameters. Other payloads that include silicon, such as logic devices, would need to be passivated with a coating to protect them from the silicon etchant.

Figure 14a presents a released out-of-plane MEMS cantilever structure while another identical cantilever can be seen

Table 3 Experimental resistance and temperature data for gold

I (mA)	Experimental R (Ω)	$\rho(\times 10^{-8})$ (1/Ω)	Experimental T (°C)
5	84.55	2.69	76.42
10	87.5	2.78	87.62
15	87.8	2.79	88.76
20	93	2.95	108.51
25	99	3.14	131.16
30	110.5	3.51	173.46
35	127	4.03	233.86
40	175	5.56	399.16
45	193	6.13	458.01

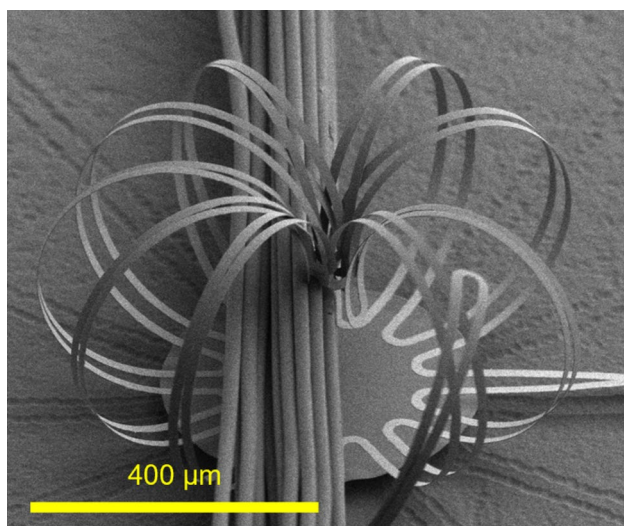


Fig. 13 SEM image of microgripper actuator claspng fiber; note the springy front arm of the gripper touching the fiber and deflecting as it makes contact

claspng onto a fiber after it had been released in Fig. 14b. The maximum horizontal extent from the attachment point of the 650 μm long cantilever is derived with and without fiber intervention through MATLAB grayscale image analysis algorithm. When the fiber is present, the cantilever is unrolled and is no longer a circle with a single radius of curvature. Since the gripper arms are making greater than 90 degree turns; the maximum horizontal extent from the attachment point is

obtained from the top view, measuring the distance between the beginning of the curling part of the cantilever and the contact pad connection of the cantilever. We have narrowed down the detection search using “Range Method” and finding the mean of the data points. Here range method is the visual estimation of the range of values for X and Y coordinates of the point of detection. This image processing algorithm was applied on 5 different SEM images. The deduced mean value of the maximum horizontal extent from the attachment point is 330 μm for images ‘with fiber’ which is greater than 137 μm obtained for images ‘without fiber’.

FEM simulation was carried out in COMSOL Multiphysics by solving a 3D curled cantilever model under applied force. The curled body of the cantilever was chosen as the point of applied force while the other end was kept fixed to monitor tip displacement (Fig. 14c). In Solid Mechanics, a point load ranging from 0 to 10 μN was applied on a node located in the curvature of the microcantilever. The cantilever was modeled in accordance with the fabricated cantilever dimensions and using original material properties provided in COMSOL material library. Figure 14d illustrates the displaced cantilever tip recorded at 330 μm under 5 μN horizontal load.

The distance from the pad to the maximum x-extent of the cantilever (the length of the green line) has approximately doubled in Fig. 14b in comparison to the one in Fig. 14a. The FEM results show the same thing happening with a 5 μN force. So, at this displacement, we can use the simulation to estimate that the cantilever is pushing back on the fiber with a 5 μN force. To further

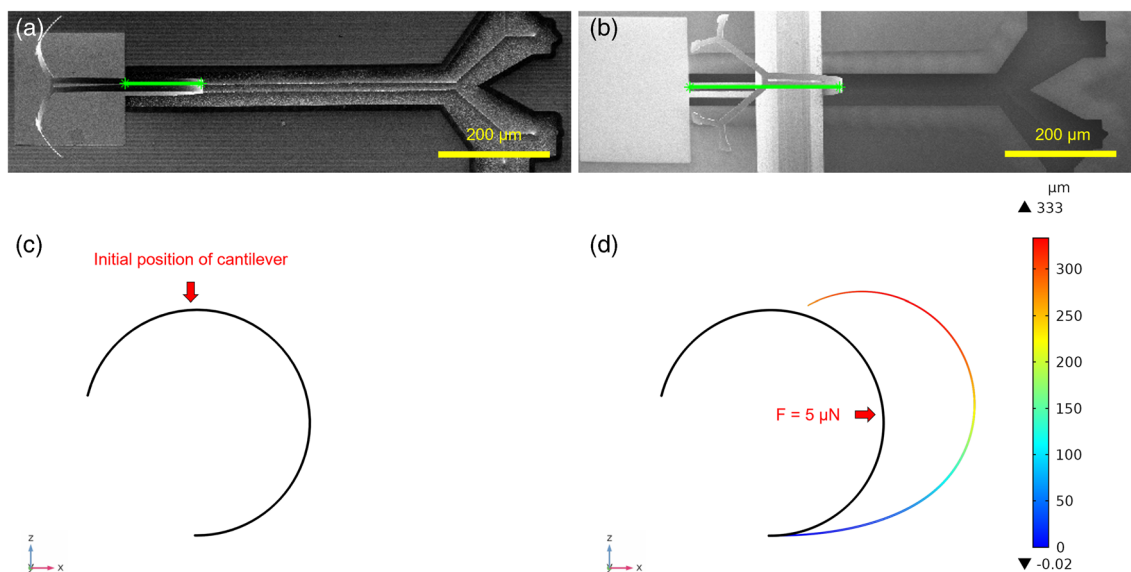
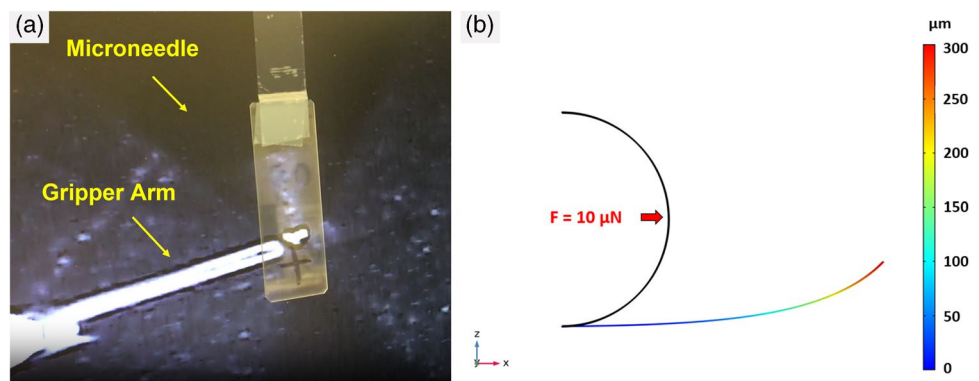


Fig. 14 SEM image of **a** released cantilever; **b** out-of-plane cantilever claspng a fiber; 3D FEM simulation of a released gripper geometry – **c** initial position of the cantilever; **d** displaced cantilever due to a 5 μN lateral applied force

Fig. 15 **a** Optical microscope image of a microgripper arm being flattened using a microneedle probe; **b** COM-SOL simulation of a bilayer microgripper arm or cantilever displaced with a $10\ \mu\text{N}$ lateral applied force



investigate the mechanical strength of these microgrippers, a microneedle probe (Dektak) was used to push one of the gripper arms vertically as shown in Fig. 15a. The probe was used to land on the fixed end of a gripper arm and then moved across its length to flatten it; upon release the gripper recovered its original shape. From our observation, $1\ \text{mg}$ or $9.8\ \mu\text{N}$ force was enough to flatten the gripper and not break it, which compares well with the result obtained through simulation. Figure 15b shows the displaced cantilever almost flattened under $10\ \mu\text{N}$ horizontal load. This information is useful for estimating the force range needed to dislodge the gripper from the fiber.

4 Conclusions

As wonderful as MEMS are, especially when merged with other technologies like ICs and/or photonics on a common substrate, one limitation is that they are made on rigid silicon substrates that do not bend or conform when attached to a soft, flexible, and at times porous substrate. This work investigated a new packaging method that relies on mechanical tangling to integrate MEMS with fibrous materials found in wearables, soft robotics, and other high-deformation applications, and also bioengineering relevant environments such as perfusable cell-growth systems that require a porous substrate for fluid access. The reversible clasping demonstrated here could potentially “program” the transfer of devices to fibrous substrates by opening all devices on a wafer and then only closing those to be transferred. Such a selective fan-out approach already makes large-area devices economically from small wafers, as seen in commercial micro-transfer printing where large-format displays are made by transferring inorganic LEDs from densely populated donor wafers. Future work on this project will investigate the grippers’ pull-off strength and electrical contact resistance, and integrate payloads before transfer.

Supplementary information The online version contains supplementary material available at <https://doi.org/10.1007/s12213-023-00161-w>.

Acknowledgements This project was supported by National Science Foundation Award 1849213, “RII Track-1: Kentucky Advanced Manufacturing Partnership for Enhanced Robotics and Structures” and National Science Foundation Award 1950137, “REU SITE: Interdisciplinary Micro/Nano/Additive Manufacturing Program Addressing Challenges Today - Next Generation (IMPACT-NG). The authors would like to acknowledge Julia Aebersold of the University of Louisville Micro/Nano Technology Center, for expertise on wire bonding devices.

Author contributions M.S.I. and S.C. wrote the main manuscript text and generated images for figures. M.S.I. and M.H.Y. designed, fabricated, and collected data on the microgrippers under the guidance of C.K.H. N.S. and D.W. fabricated and collected data by testing the cantilevers. S.S.V. and S.C. prepared Table 2; Fig. 13 (a, b). N.S. prepared Fig. 8. Finite Elements Analysis was performed by M.S.I. S.C. and M.S.I. prepared Tables 3 and 4. J.B. assisted in the microfabrication processing of the MEMS devices. All authors reviewed the manuscript.

Funding This project was supported by National Science Foundation Award 1849213, “RII Track-1: Kentucky Advanced Manufacturing Partnership for Enhanced Robotics and Structures” and National Science Foundation Award 1950137, “REU SITE: Interdisciplinary Micro/Nano/Additive Manufacturing Program Addressing Challenges Today - Next Generation (IMPACT-NG).

Data availability Not applicable.

Declarations

Competing interests The authors declare no competing interests.

References

1. Harnett CK, Moiseeva EV, Casper BA, Wilson LJ (2010) Microscopic containers for sample archiving in environmental and biomedical sensors. In: 2010 IEEE Instrumentation & Measurement Technology Conference Proceedings. IEEE, pp 328–331
2. Lucas TM, Porter DA, Beharic J, Berfield TA, Harnett CK (2017) Bistability in a symmetric out-of-plane microstructure. *Microsyst Technol* 23(7):2569–2576

3. Martin-Olmos C, Rasool HI, Weiller BH, Gimzewski JK (2013) Graphene MEMS: AFM probe performance improvement. *ACS Nano* 7(5):4164–4170
4. Challa S, Islam MS, Harnett CK (2019) Fiber-crawling micro-robots. In: 2019 International Conference on Manipulation, Automation and Robotics at Small Scales (MARSS), Helsinki, Finland, pp 1–6. <https://doi.org/10.1109/MARSS.2019.8860986>
5. Ghazali AM, Hasan MN, Rehman T, Nafea M, Ali MSM, Takahata K (2020) MEMS actuators for biomedical applications: a review. *J Micromech Microeng* 30(7):073001
6. Agcayazi T, Chatterjee K, Bozkurt A, Ghosh TK (2018) Flexible interconnects for electronic textiles. *Adv Mater Technol* 3(10):1700277
7. Wei D, Challa S, Islam MS, Beharic J, Harnett CK, Popa DO (2022) Multi-robot collaboration for electronic textile fabrication, 2022 International Conference on Manipulation, Automation and Robotics at Small Scales (MARSS), pp. 1–6. <https://doi.org/10.1109/MARSS55884.2022.9870470>
8. Wang S, Huang Y, Rogers JA (2015) Mechanical designs for inorganic stretchable circuits in soft electronics. *IEEE Trans Compon Packaging Manuf Technol* 5(9):1201–1218
9. Hillmer H et al (2018) Optical MEMS-based micromirror arrays for active light steering in smart windows. *Jpn J Appl Phys* 57(8S2):08PA07
10. Zhu Y, Pal J, “Erratum: Zhu Y, Pal J (2021) Low-voltage and high-reliability RF MEMS switch with combined electrothermal and electrostatic actuation. *Micromachines* 12, 1237. *Micromachines* (Basel) 12(11, Nov. 2021). <https://doi.org/10.3390/mi12111389>
11. Lv X, Wei W, Mao X, Chen Y, Yang J, Yang F (2015) A novel MEMS electromagnetic actuator with large displacement. *Sens Actuators A Phys* 221:22–28
12. Conway NJ, Traina ZJ, Kim S-G (2007) A strain amplifying piezoelectric MEMS actuator. *J Micromech Microeng* 17(4):781
13. Cauchi M, Grech I, Mallia B, Mollicone P, Sammut N (2019) The Effects of Cold Arm Width and Metal Deposition on the performance of a U-Beam Electrothermal MEMS Microgripper for Biomedical Applications. *Micromachines* (Basel) 10(3). <https://doi.org/10.3390/mi10030167>
14. Ziko MH, Koel A (2018) Theoretical and numerical investigations on a silicon-based MEMS chevron type thermal actuator. In: 2018 IEEE 18th International Conference on Nanotechnology (IEEE-NANO). IEEE, pp 1–5
15. Algamili S et al (2021) A review of actuation and sensing mechanisms in MEMS-based sensor devices. *Nanoscale Res Lett* 16(1):16
16. Challa S, Ternival C, Islam S, Beharic J, Harnett C (2019) Transferring microelectromechanical devices to breathable fabric carriers with strain-engineered grippers. *MRS Adv* 4(23):1327–1334. <https://doi.org/10.1557/adv.2019.6>
17. Sonker MK (2015) Design and simulation of Tri-morph based MEMS thermal sensor for harsh environment. In: 2015 International Conference on Computer, Communication and Control (IC4). IEEE, pp 1–7
18. Xu T-B, Su J, Zhang Q (2003) Electroactive-polymer-based MEMS for aerospace and medical applications, in smart structures and materials 2003: smart electronics, MEMS, BioMEMS, and nanotechnology. Jul 5055:66–77
19. Jia K, Pal S, Xie H (2009) An electrothermal Tip-Tilt-Piston micromirror based on folded dual S-Shaped bimorphs. *J Microelectromech Syst* 18(5):1004–1015. <https://doi.org/10.1109/JMEMS.2009.2023838>
20. Zhang X, Li B, Li X, Xie H (2015) A robust, fast electrothermal micromirror with symmetric bimorph actuators made of copper/tungsten. In: 2015 Transducers-2015 18th International Conference on Solid-State Sensors, Actuators and Microsystems (TRANSDUCERS). IEEE, pp 912–915
21. Goessling BA, Lucas TM, Moiseeva EV, Aebersold JW, Harnett CK (2011) Bistable out-of-plane stress-mismatched thermally actuated Bilayer Devices with large deflection. *J Micromech Microeng: Struct Devices Syst* 21(6):065030
22. Boyes W (ed) (2010) Instrumentation reference book, 4th edn. Butterworth-Heinemann/Elsevier, Boston
23. Prasad M, Dutta PS (2018) Development of Micro-Hotplate and its reliability for gas sensing applications. *Appl Phys A Mater Sci Process* 124(11):788

Publisher’s note Springer Nature remains neutral with regard to jurisdictional claims in published maps and institutional affiliations.

Springer Nature or its licensor (e.g. a society or other partner) holds exclusive rights to this article under a publishing agreement with the author(s) or other rightsholder(s); author self-archiving of the accepted manuscript version of this article is solely governed by the terms of such publishing agreement and applicable law.